

KINEMATICS AND MUSCLE DYNAMICS OF C- AND S-STARTS OF CARP (*CYPRINUS CARPIO* L.)

IGOR L. Y. SPIERTS^{1,*} AND JOHAN L. VAN LEEUWEN^{2,3}

¹Experimental Zoology Group, WIAS (Wageningen Institute of Animal Sciences), Wageningen Agricultural University, NL-6709 PG Wageningen, The Netherlands, ²Department of Physiology, Leiden University, Wassenaarseweg 62, PO Box 9604, NL-2300 RC Leiden and ³Institute of Evolutionary and Ecological Sciences, Leiden University, Kaiserstraat 63, PO Box 9516, NL-2300 RA Leiden, The Netherlands

*e-mail: Igor.Spierts@morf.edc.wau.nl

Accepted 23 November 1998; published on WWW 21 January 1999

Summary

An analysis is presented of body curvature, acceleration and muscle strain during fast-starts in the common carp (*Cyprinus carpio* L.). C- and S-starts were filmed at 200 frames s⁻¹ at 23 °C. Curvatures and accelerations of mid-body axes were calculated from digitised outlines. Maximum accelerations at 0.3 FL (fork length) from the snout were 54 m s⁻² for C-starts and 40 m s⁻² for S-starts. The total turning angle was approximately 150° in C-starts. This angle was 70° during escape S-starts, significantly larger than for predatory S-starts in other species. Sarcomere strains of axial muscle fibres were calculated at 0.4 and 0.8 FL. During C-starts, white muscle fibres were exposed to maximum sarcomere strains of up to approximately 16%, and posterior fibres had similar strains to anterior fibres (red 27%; white 16%). During S-starts, however, maximum strains in anterior fibres (red 39%; white 24%) were more than twice those in posterior

fibres (red 17%; white 10%). In a C-start, the fish made a large turning angle directed away from the stimulus by bending its tail strongly and thereby producing a large thrust. A larger anterior peak curvature of the fish during S-starts enabled the carp to control the direction of escape better than during C-starts, but with lower accelerations and smaller turning angles. During cyclic and intermittent swimming, red posterior fibres experienced the largest strains. Interestingly, previous studies have shown these fibres to have the lowest passive stiffness and the largest titin isoform, allowing them to attain large strain amplitudes with relatively low passive tensions.

Key words: red muscle, white muscle, startle response, C-start, S-start, intermediate swimming, acceleration, body curvature, turning rate, sarcomere, titin, carp, *Cyprinus carpio*.

Introduction

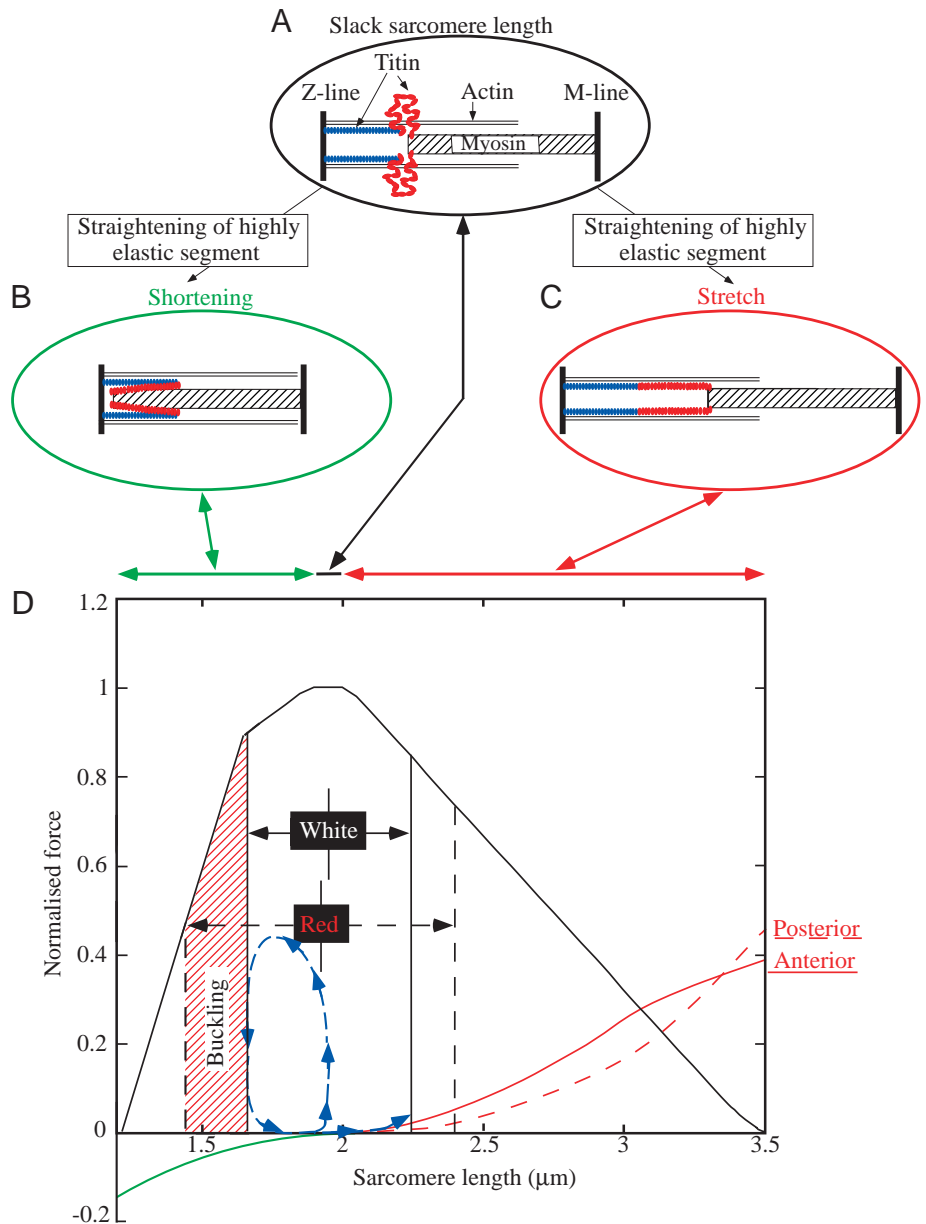
Fish generate fast-start swimming manoeuvres to avoid predators and to capture prey. Very high accelerations of the body (typically 30 m s⁻² or more, see Domenici and Blake, 1997) enable high swimming velocities to be attained in a short time. Three kinematic stages of fast-starts have been described: (1) a preparatory stroke; (2) a propulsive stroke; and (3) a subsequent variable behaviour (Weihs, 1973; Webb, 1976; Webb and Blake, 1985). For subcarangiform swimming (in teleosts), two major types of fast-start, generally referred to as C- and S-starts, have been distinguished (Hertel, 1966; Weihs, 1973; Eaton et al., 1977; Webb, 1975, 1976, 1978a,b; Webb and Blake, 1985). During C-starts, the whole trunk curves in the same direction (Weihs, 1973; Webb, 1978a; Frith and Blake, 1991). These escape or startle responses are usually mediated by the Mauthner system (Eaton et al., 1977; Kimmel et al., 1980). C-starts have been subdivided into single- and double-bend types, depending on the presence of a second tail beat (Domenici and Blake, 1991; Kasapi et al., 1993).

S-starts have been subdivided into those occurring during

predatory attacks and escape responses. During predation starts, the turning angle of the body is small and the posterior region of the trunk curves more than the anterior portion (Hoogland et al., 1956). S-shaped escape responses exist with considerable turning angles (generally smaller than in C-starts). Little is known about the neuronal mechanisms controlling S-starts.

Kinematic analyses of fast-starts of fish provide important information (e.g. curvature of the fish body and acceleration of the fish) for a functional analysis of the axial muscles that drive the movements. The lateral curvature of the fish body can be used to derive the length changes of the sarcomeres. The tensile stresses of the sarcomeres are strain-dependent owing to length-dependent variations in (1) the overlap of thick and thin filaments (active contribution) and (2) the tension of titin (passive). Titin, a giant highly elastic muscle protein, is a stabilising structure that spans the distance between the Z- and M-lines of the sarcomere and contributes importantly to passive tension (Fig. 1). The titin segment in the A-band region

Fig. 1. Hypothesised mechanism of passive tension generation by titin (schematic). The titin segment in the A-band region of the sarcomere is ignored in this figure for the sake of clarity. The I-band segment of titin consists of two subsegments: a stiff anchoring segment attached to the Z-line (coloured blue) and a highly elastic segment, connecting the anchoring segment to the myosin filaments (coloured red). (A) Slack sarcomere. The highly elastic titin segment is highly folded. (B) Sarcomere shortened below the slack length. The highly elastic segment of titin straightens and passive tension develops (see corresponding green curve in D). (C) Sarcomere stretch. The highly elastic segment of titin again straightens and passive tension develops (see corresponding red curves in D). (D) Force–sarcomere length curve for carp red and white muscles. The lengths of the actin and myosin filaments are $1.82\ \mu\text{m}$ and $1.58\ \mu\text{m}$, respectively. The passive tension *versus* sarcomere length curves for carp red anterior and posterior fibres upon stretching (red curves) and shortening (green curve), derived from the data of Spierts et al. (1997), are also shown and are expressed relative to a maximum active tension of approximately 150 kPa. The mean maximum sarcomere length excursions of red (25.1%) and white (14.7%) axial muscle fibres during fast-starts are indicated by dashed and solid lines, respectively. The blue dashed line indicates a hypothetical work loop for the white muscles that primarily power fast-starts and generate approximately 50% maximum tension. During (passive) muscle lengthening, the work loop ‘follows’ the matching passive tension *versus* sarcomere length curve (not indicated for white muscles; see text for further details). Red fibres are not able to keep up with the high shortening velocity of white fibres and therefore tend to buckle at the concave side of the fish body (see red hatched area). A–C are based on Granzier et al. (1996).



of the sarcomere is ignored in this figure for the sake of clarity. Titin also helps to maintain the central position of thick filaments in contracting sarcomeres (Wang, 1985; Maruyama, 1986, 1994; Wang et al., 1991, 1993; Fürst et al., 1988; Granzier et al., 1996).

So far, very few studies have investigated the strain waves during intermittent swimming, turning manoeuvres and fast-starts. van Leeuwen et al. (1990) recorded high-speed film of carp (*Cyprinus carpio*) during cyclic and kick-and-glide swimming simultaneously with electromyographic recordings of the slow muscle fibres at eight positions along the trunk. The strain and strain rate of the slow fibres were determined (using curvature data) and used to calculate the force and power

output of the muscle fibres. For kick-and-glide swimming, van Leeuwen et al. (1990) found that intermediate and fast muscle fibres are required to drive the movements.

Rome et al. (1988) examined strain rate amplitudes of fast and slow fibres during fast-starts in carp (*Cyprinus carpio*). These data were compared with experimentally obtained values for maximum shortening speed, and they suggested that fast fibres operated at strain rates close to optimum values for maximum power output.

Johnston et al. (1995) investigated instantaneous muscle strain and power output during a fast-start in the short-horned sculpin (*Myoxocephalus scorpius*). Predation fast-starts were filmed, and muscle strains were calculated for dorsal fast

muscle using the lateral body curvature and the fibre orientation. The maximum peak-to-peak ranges of the muscle strain at 15 °C during the first tail beat were largest (approximately 0.19) at 0.52 *TL* (where *TL* is the total length of the fish measured from the snout) and smallest (approximately 0.15) at 0.77 *TL*. At 0.32 *TL*, the muscle strain range was 0.16. Furthermore, fibres at 0.52 *TL* and 0.77 *TL* on the same side of the body were initially stretched by the contralateral bending of the fish body, thus receiving a pre-stretch prior to shortening.

The present study examines fast-starts in carp. First, we will quantify the kinematic profiles of C- and S-starts by measuring and calculating (1) turning angles of the anterior part of the body, (2) accelerations at 0.3 *FL*, and (3) lateral body curvature as a function of position and time. Second, the curvature data and measured muscle fibre orientations are used to calculate strain variations of anterior and posterior red and white axial muscle fibres. Finally, sarcomere strains are used to interpret known structural features of the sarcomeres (which vary with fibre type and position along the trunk), such as the dimensions of titin and myofilaments.

Materials and methods

Swimming experiments

Eight specimens of common carp (*Cyprinus carpio* L.), 22.5–27.5 cm in fork length (*FL*), bred in the laboratory at 23 °C and fed on commercial fish food (Trouvit pellets; Trouw and Co. Putten) were used. High-speed motion films were made to determine sarcomere length changes (muscle strain) during fast swimming at 0.4 and 0.8 *FL* (measured from the snout) in red and white axial muscle fibres of carp. Swimming events of the fish were filmed from a dorsal viewpoint in a tank (90 cm long, 45 cm wide and 45 cm deep) using a Teledyne DBM 54 16 mm high-speed ciné camera at 200 frames s^{-1} . The camera was positioned 2 m above the tank, and a Nikon 28 mm lens was used to capture images of the complete tank. Films (Kodak double-X negative, 250 ASA) were taken with continuous light from seven Hama video lights so as to obtain sharp silhouettes of the swimming fish (power input of 5.2 kW). Water temperature was 23 °C, and warming of the aquarium by the filming lights was negligible because of the short lighting periods. Fast swimming responses, C- and S-starts and an intermediate swimming mode (I-swimming) were elicited by a sudden sound wave in the tank created by a blow to the laboratory floor adjacent to the tank or by tapping the side of the tank with a hard rubber mallet.

Calculation of accelerations and muscle fibre strain

Films were analysed by projecting them onto sheets of A3 paper through a flat glass plate. Projected outlines of the fish during fast-starts and cyclic swimming were traced onto the paper at 5 ms intervals and digitised relative to fixed reference points, using an *x,y*-data tablet (Calcomp 9100). For each side of the body, approximately 100 points were used. The points were distributed non-equidistantly. The shortest distances were used for the strongest curvatures of the outline. The estimated

maximum error of the digitising process was 0.5 mm, which is approximately 0.002 % of the fork length of the fish.

For successive frames, a longitudinal axis of the fish during the swimming event was calculated from its digitised outlines, using the methods of van Leeuwen et al. (1990) and Johnston et al. (1995). The axis was divided into a number (typically 20–35) of straight-line segments before its shape was calculated. The mathematical segment length Δs was reduced linearly down the trunk of the fish:

$$\Delta s = \frac{(FL-s)s_1 + ss_2}{FL}, \quad (1)$$

where *FL* is the fork length of the fish (determined independently for the fish in a straight position), *s* is the distance of the most rostral point of the segment along the axis from the snout, *s*₁ is the length of the most rostral segment, and *s*₂ is a second prescribed length (*s*₂ < *s*₁). The variable segment length improved the stability of the applied algorithm while approaching the actual curvatures as closely as possible by allowing enough flexibility. The largest segment length chosen was in the head region, which is very stiff, allowing practically no curvature (typically *s*₁ ≈ 0.1 *FL*) and the smallest segment length was in the tail region where curvature is largest (typically *s*₁ ≈ 0.025 *FL*). The chosen segment lengths corresponded approximately to the anatomical length of the carp segments (skull, vertebrae and finray segments, respectively). Every axis was calculated starting at the anteriormost visible point of the body (determined manually). The orientation of each new axis segment was found iteratively by assuming that the left and right projected fish areas were equal (van Leeuwen et al., 1990). This assumption was supported by the results of radiography of free-swimming fish (van Leeuwen et al., 1990). The axis calculation ended at the posteriormost visible point of the body (i.e. the fork point of the tail blade, also determined manually).

The number of initial segments was allowed to vary from frame to frame (generally, the highest numbers of segments were used for the strongest curvatures). The 'raw' data were therefore interpolated so as to obtain 31 points for each calculated axis. The axes were subsequently smoothed as a function of position down the trunk using natural cubic *B*-spline functions (spline function package; Woltring, 1986). A natural spline function can be defined as a piecewise polynomial function between and outside selected knot positions *s*_{*j*} on the abscissa (reflecting, for the positional smoothing, the distances along the axis to the anterior snout point). A *B*-spline (e.g. de Boor, 1978) of degree *q* consists of *q*+1 polynomial pieces that join at *q* inner knots. Derivatives up to order *q*−1 are continuous at the joining points. On a basis of *B*-splines *B*_{*j*}(*s*): *j*=1, ..., *n*, a fitted spline curve \hat{w} to data (*s*_{*j*}, *w*_{*j*}) is the linear combination:

$$\hat{w} = \sum_{j=1}^n \hat{a} B_j(s, q), \quad (2)$$

where \hat{a} are the spline coefficients. The spline coefficients can be manipulated using the so-called regularisation or smoothing

parameter (Woltring, 1986). For smoothing of the axes, appropriate values were chosen for the smoothing parameter (the higher the smoothing factor, the more 'straight' the curve approximation becomes) in such a way that (1) the fish axis was kept as straight as possible in the head region, (2) unrealistic small-scale fluctuations (i.e. with a length of the order of a few anatomical segments of the fish) in the curvature were eliminated, and (3) the fundamental characteristics of the wave of lateral curvature were preserved (i.e. over-smoothing was avoided). A more objective smoothing criterion, such as the minimisation of the generalised cross-validation (GCV, for details, see Woltring, 1986) function, could not be used for the positional smoothing because of correlated errors in neighbouring points. This would lead to too small a smoothing parameter. The smoothed axes (x_p, y_p) were described in parametric form by $x_p=F(s,t)$ and $y_p=G(s,t)$, where t is time, and F and G are functions. Owing to inaccuracies in the digitising process (see above), small errors were introduced that varied from frame to frame, such as very small undesired rigid body displacements and rotations. Functions x_p and y_p were therefore smoothed as a function of time using quintic natural B -spline functions and the GCV criterion as described by Woltring (1986). The GCV criterion was used because the mean squared error in the data was not known *a priori*. The GCV criterion should be used cautiously because it leads to under-smoothing if too small a number of knots is used for a given knot density (our data sets contained several hundred points, far more than the minimum number of 40 suggested in Woltring, 1986, which was evaluated to be too low). This last smoothing step had only a minor effect on the data set. The calculated axes (using the smoothed 31 points per frame) were used to calculate the turning rates (degrees ms^{-1}) of the midline of the anterior part of the body (snout to estimated centre of mass at $0.3 FL$) throughout a C- and an S-start. We also calculated the accelerations (derived as the rate of change of the velocity magnitude in time) of some carp at $0.3 FL$ during C- and S-starts.

The absolute curvature k was calculated using the F and G functions introduced above in the following formula (Lipschutz, 1969):

$$k = \frac{\sqrt{\left(\frac{d^2F}{ds^2}\right)^2 + \left(\frac{d^2G}{ds^2}\right)^2}}{\left(\frac{dF}{ds}\right)^2 + \left(\frac{dG}{ds}\right)^2}. \quad (3)$$

The fork length divided by the local radius of the curvature R gave the normalised curvature (FL/R), which is defined as positive for curvature to the right and as negative for curvature to the left. For reasons similar to those given for the accelerations, the curvatures obtained from the $x_p(s,t)$ and $y_p(s,t)$ data were finally smoothed as a function of time using the GCV criterion. In calculating the strain, the observed thickening at the concave side of the body, the thinning at the convex side and the position and orientation of the muscle fibres were taken into account. It was assumed that the fibres were at their resting length when the trunk was straight. The

strain ϵ_{paq} in a direction parallel to the axis, at an instantaneous distance d from the median plane, was calculated as (van Leeuwen et al., 1990):

$$\epsilon_{\text{paq}} = -\frac{d}{R} \quad (4)$$

for the concave side of the body, and

$$\epsilon_{\text{paq}} = \frac{d}{R} \quad (5)$$

for the convex side of the body, where $R=1/k$ is the local radius of curvature. Similarly, the strain ϵ_{ppq} perpendicular to the axis, at an instantaneous distance d from the median plane, was calculated as (van Leeuwen et al., 1990):

$$\epsilon_{\text{ppq}} = \frac{R}{\sqrt{(R-2d_0)R}} - 1 \quad (6)$$

for the concave side of the body, and

$$\epsilon_{\text{ppq}} = \frac{R}{\sqrt{(R+2d_0)R}} - 1, \quad (7)$$

for the convex side of the body, where d_0 is the corresponding (initial) distance in the straight axis position. Finally, the strains of red and white muscle fibres were calculated using:

$$\epsilon_p = l^2 \epsilon_{\text{ppq}} + n^2 \epsilon_{\text{paq}}, \quad (8)$$

where l and n are the direction cosines of the muscle fibres in the perpendicular and the parallel direction, respectively.

Eight fish were used for the strain calculations and, for every fish, C-starts, S-starts and a fast-swimming mode intermediate between these two forms (I-swimming) were filmed and digitised. In total, we used 24 filmed scenes of fast-starts. Using equations 4–7, the maximum sarcomere strains were calculated for red and white muscle fibres at 0.4 and $0.8 FL$ for all fast-starts examined. For every type of fast-start, a mean maximum sarcomere strain was calculated for each muscle type and location (i.e. the mean of eight maximum values, one per filmed scene).

We also examined mean sarcomere strains during cyclic swimming of each carp. All computer programs were written for the Macintosh family of computers, using Think Pascal 4.0.2 (Symantec Corp.) or Mac FORTRAN II (Absoft Corp.) as programming languages. The two-dimensional-curvature data were interpolated using the cubic interpolation routine available in the Transform plotting package (Fortner Research LLC). The interpolated data were represented as contour plots.

The calculations did not compensate for possible buckling effects that are likely to occur in the red fibres during fast-starts. Unrealistically low negative sarcomere strains for red muscles were therefore obtained occasionally (see Results and Discussion). Only positive strains of the sarcomere (on both the left and right sides of the body during a filmed scene) were included in the statistical analysis.

Muscle fibre orientation and sarcomere length measurements

The red and white muscle fibre position and orientation were measured using the method described by Alexander (1969). The skin of the fish was removed from one side of the body to reveal the musculature, and incisions were made using a sharp razor blade at the mid-point of the red (1–2 mm deep) and dorsal white muscle (3–4 mm deep) at points 0.4 and 0.8 *FL* along the body (Fig. 2). The angles, measured with respect to the median and frontal plane of the fish, were used to correct strain calculations for the orientation of red and white fibres.

Red and white muscle fibres at 0.4 *FL* and 0.8 *FL* along the trunk of a carp were prepared for electron microscopy as described by Akster (1985). The length of the actin filament and the myosin filament were measured. We used the cross striation in the I-band (caused by the 38.5 nm periodicity of the troponin complexes on the actin filament; Page and Huxley, 1963) to correct for the combined effects of uncertainties in the microscopic magnification and shrinkage. In this way, the natural length of the filaments could be accurately determined. In addition, our filament length measurements and derived sarcomere resting length were supported by single-fibre laser diffraction length measurements and force measurements (Spierts et al., 1997).

Statistics

The maximum strain data calculated in this study (relative

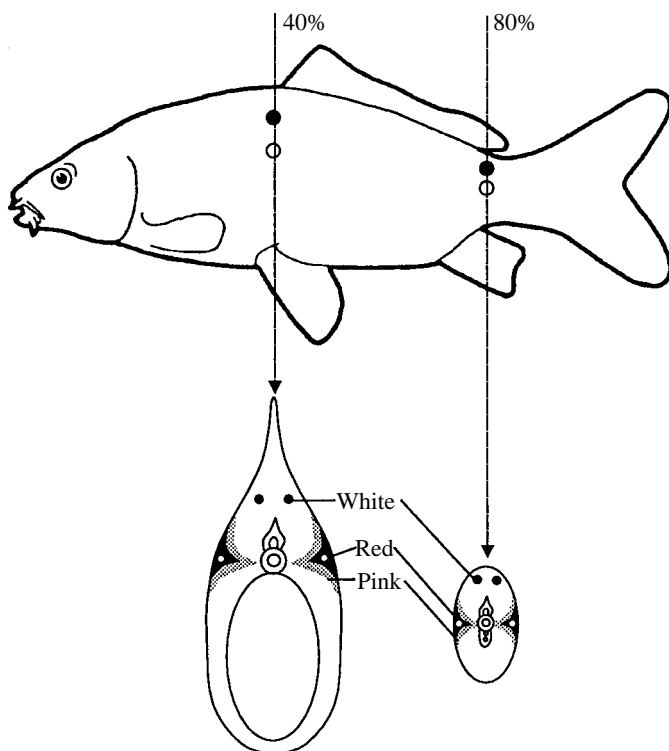


Fig. 2. Schematic drawing showing the positions used for calculating the muscle fibre strain in red and white muscle tissue on the left and right side of the fish body at 0.4 and 0.8 *FL*, where *FL* is fork length. The positions for white and red muscle tissue are indicated by filled and open circles, respectively.

values) appeared to be normally distributed (Shapiro and Wilk, 1965). The differences in sarcomere strain we found between red and white anterior and posterior muscle fibres during different swimming modes were analysed statistically using a univariate analysis of variance procedure (ANOVA; SAS 6.11, SAS Institute Inc., Cary, USA), *t*-tests and least significant difference (LSD) of means (Sokal and Rohlf, 1981). Individual fish were taken as a random factor with four test positions of sarcomeres. Statements of statistical significance are based on $P \leq 0.05$ unless specified otherwise (Sokal and Rohlf, 1981; Rohlf and Sokal, 1981). Values are presented as means \pm s.d.

Results

The ranges of muscle fibre angles measured with respect to the median planes were 4–6° at 0.4 *FL* and 6–8° at 0.8 *FL* for red muscle fibres, and 20–27° at 0.4 *FL* and 12–17° at 0.8 *FL* for white muscle fibres. The ranges of angles measured with respect to the frontal plane were 8–10° at 0.4 *FL* and 2–5° at 0.8 *FL* for red muscle fibres, and 14–16° at 0.4 *FL* and 29–31° at 0.8 *FL* for white muscle fibres. The mean sarcomere lengths of red fibres, $1.95 \pm 0.0032 \mu\text{m}$, and of white fibres, $1.92 \pm 0.0036 \mu\text{m}$, differed significantly ($N=36$). The length of the actin filament was $1.82 \pm 0.028 \mu\text{m}$ ($N=12$) and the length of the myosin filament was $1.58 \pm 0.041 \mu\text{m}$ ($N=12$). As values varied very little along the trunk, no significant differences were found between anterior and posterior fibres.

Three types of fast-starts were distinguished: a typical C-start or startle response, an S-start and an intermediate fast-swimming mode (I-swimming). The statistical analysis did not reveal significant differences between individual fish.

Swimming responses of carp after introducing a sound wave into the tank

C-start

C-starts of carp occurred very suddenly and rapidly and involved large turning angles. Fig. 3 is an example of a single-bend C-start showing the calculated central axis of an adult carp (Fig. 3A) and the turning rate of the anterior body midline (Fig. 3B). Only stage 1 could be recognised, which is typical for a single-bend C-start because no change in turning direction occurs. Stage 1 started at $t=0$ ms, when the carp was in a resting position, and ended at $t=100$ ms, when the turning rate had decreased to zero. The maximum turning rate was 4°ms^{-1} . After 100 ms, a total turning angle of 155° had been reached. Fig. 3C shows a contour plot of the body curvature during this C-start. The horizontal axis represents the normalised position along the body axis (0=tip of snout, 1=fork of tail fin), the ordinate shows the time, and the colours and contours in the plot show the normalised curvature FL/R (R is the local radius of curvature). The largest curvatures occurred between 0.5 and 0.8 *FL*. The body bent mainly to the right side during this start, although between 0 and 20 ms a very small curvature to the left was calculated for the tail region. At approximately 0.6 *FL*, the maximum curvature (inner small contour in the red area) was reached approximately 25 ms after starting from an almost

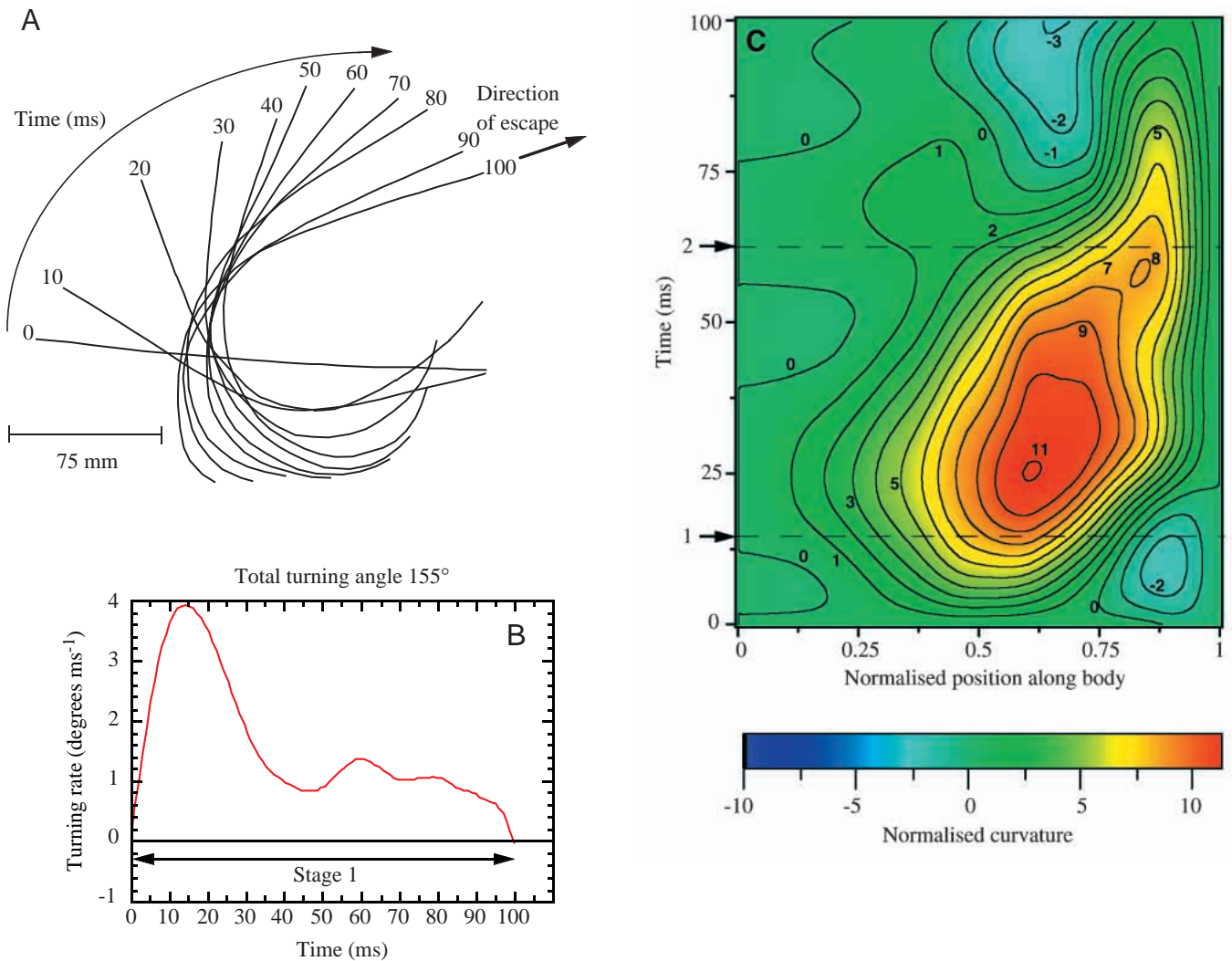


Fig. 3. Single-bend C-start of an adult carp. (A) The central axis of the fish (plotted using the 31 points derived per calculated axis) during a single-bend C-start, shown every 10 ms. Times between tracings are in milliseconds from the first detectable movement. (B) The turning rate of the anterior body midline (snout to estimated centre of mass at $0.3FL$, where FL is fork length) during this C-start. The single-bend C-start consisted of stage 1 only. (C) Contour plot of the body curvature during this C-start. The horizontal axis represents the body axis of the fish expressed as normalized FL (0 =tip of snout, 1 =fork of tail fin), the ordinate shows the time, and the colours and contours in the plot show the normalized curvature FL/R (where R is the local radius of curvature). Curvature was positive for bending to the right and negative for bending to the left. The dashed horizontal reference lines numbered 1 and 2 indicate the peaks in acceleration of the fish axis at $0.3FL$ during this C-start, shown in Fig. 4A.

straight position. The contours show that the position of peak curvature along the trunk travelled at fairly constant speed from 0.5 to $0.72FL$ (approximately $5FLs^{-1}$). Between 0.72 and $0.85FL$ (peduncle region), the speed of the position of peak curvature was much higher, and the speed dropped again in the most posterior region.

Fig. 4A,B shows two typical examples of the acceleration of the fish axis at $0.3FL$ during a C-start. Fig. 4A is from the same start as shown in Fig. 3. In the first 20 ms of a C-start, large accelerations of up to $54ms^{-2}$ were achieved. The acceleration during a C-start showed at least two peaks. The first main peak almost coincided with the moment of maximum turning rate (Fig. 3B), just before the moment of maximum curvature. The timing of peaks 1 and 2 (Fig. 4A) is indicated by dashed horizontal lines in Fig. 3C.

The curvatures of the fish (Fig. 5A–C) clearly showed that both head and tail region curved extensively in the same direction during the C-start, resulting in large sarcomere strains anteriorly as well as posteriorly. In Fig. 5A, the carp started from a straight position. In Fig. 5B,C, the fast-start began while the fish was swimming slowly. In these latter cases, the fast-start was preceded by a short preparatory stroke (see the first 10–15 ms) owing to the preceding swimming motion. During this stroke, the fish body bent slightly, after which the large C-shape developed in the opposite direction. Fish often performed double-bend C-starts, which consisted of two stages (e.g. Fig. 5A–C). During stage 1, the carp bent extensively to one side, followed by a smaller bend to the opposite side, stage 2. In the absence of electromyographic (EMG) recordings, stages 1 and 2 of a fast-start were defined using the turning rate

(Figs 3B, 6B). Stages 1 and 2 were delimited by the changes in the turning direction of the anterior body midline (after Domenici and Blake, 1991, 1993b; Kasapi et al., 1993). The double-bend C-starts investigated lasted approximately 50–100 ms (the sum of stages 1 and 2). When carp performed C-starts, the maximum curvature on one side of the body (anteriorly, posteriorly or both) was always reached within 10–25 ms after starting from a straight body position. During this period of maximum curvature, maximum sarcomere strains were reached on the convex side of the fish body (see Figs 7A–C, 8A–C). Anterior and posterior maximum curvatures were reached with a time difference up to approximately 5 ms (Fig. 5A–C).

S-start

Fig. 6 is an example of an S-start showing the central axis of an adult carp (Fig. 6A) and the turning rates of the anterior body midline (Fig. 6B). In stage 1, the carp started from a straight position and bent into a large S-shape with turning rates up to approximately 1.5°ms^{-1} . At $t=60$ ms, the turning rate became negative and stage 1 was followed by stage 2, in which the fish adopted an opposite S-shape. Stage 2 lasted until approximately $t=88$ ms, when a further reversal of turning direction occurred and stage 3 (variable behaviour) followed. At 140 ms, the total turning angle was 72° . Fig. 6C shows a contour plot of the body curvature during this S-start. The contour plot shows that at each instant positive and negative curvatures were present down the trunk, which is typical for an S-start. The largest curvature

occurred at $0.5 FL$ (dark blue area) and was reached approximately 50 ms after the initial straight position. The contours show that the position of maximum curvature along the trunk travelled at fairly constant speed from 0.35 to $0.7 FL$ (approximately $10 FL s^{-1}$). In contrast to the C-start of Fig. 3, the speed decreased gradually posteriorly from $0.7 FL$. These were typical S-starts because the largest curvatures occurred approximately half-way along the trunk (resulting in large anterior sarcomere strains, see below). S-starts of carp occurred at lower accelerations (Fig. 4) than in C-starts with displacements that were more in line with the body axis. Fig. 4C,D shows two typical examples of the acceleration of the fish at $0.3 FL$ during S-starts. In the S-start shown in Fig. 4C, the fish began the movement slowly, after which large accelerations occurred (peak close to 40 m s^{-2}). The peaks in the acceleration curve (in Fig. 4C at $t=45$ ms and in Fig. 4D at 15 ms and 70 ms) coincided with moments at which the tail fin had a high lateral velocity (approximately $3\text{--}4 \text{ m s}^{-1}$) and was at a considerable angle (approximately $70\text{--}90^\circ$) relative to the direction of movement (i.e. favourable conditions for generating thrust).

The normalised curvatures plotted in Fig. 5D,F are for fish that began the S-start while swimming slowly, whereas in Fig. 5E the fish was in a straight position at the beginning of the start. The S-starts investigated lasted slightly longer (stages 1+2) than the C-starts, and lower turning rates were achieved. The time carp required to reach maximum curvature from a straight position (with large strains, see Figs 7D–F, 8D–F) was longer and more variable than in the C-starts.

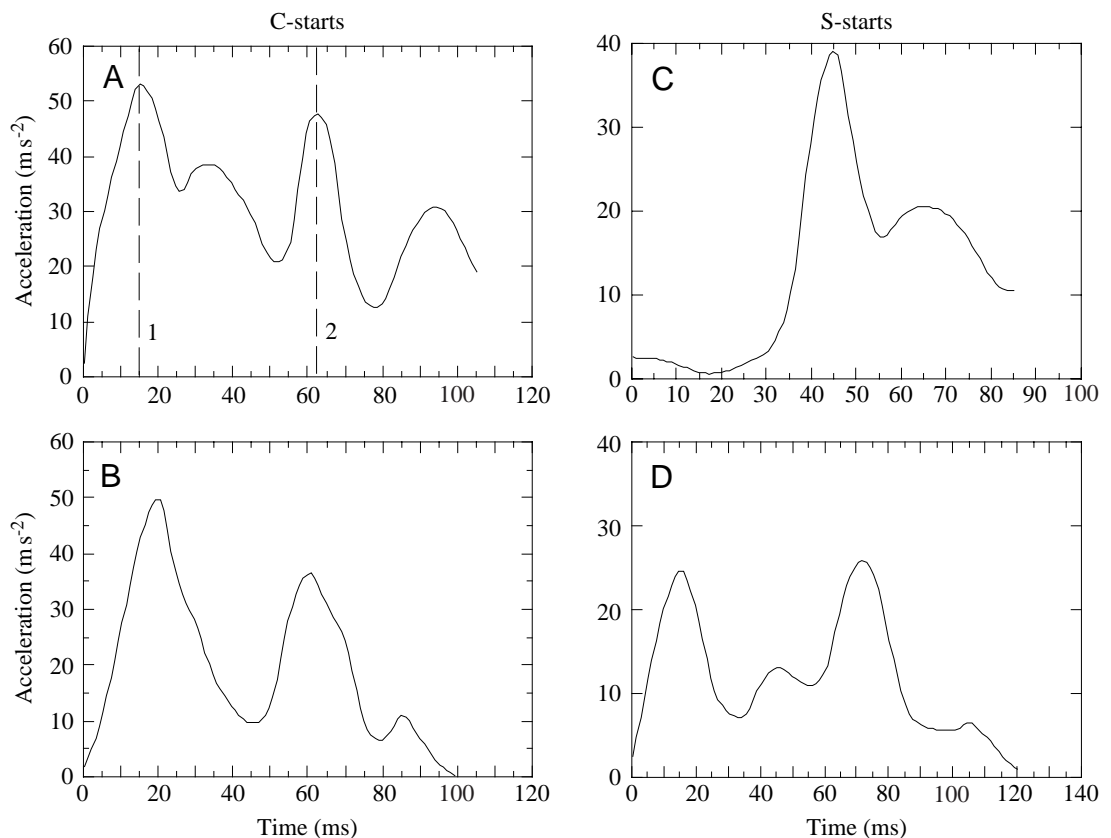


Fig. 4. Typical examples of acceleration (derived from velocity data) of the fish axis at $0.3 FL$, where FL is fork length, during fast-starts. (A,B) C-starts. A represents the start shown in Fig. 3. The timings of the two peaks of acceleration in A, labelled 1 and 2, are indicated by the dashed horizontal lines in Fig. 3C. (C,D) S-starts. C shows a slow start followed by a large acceleration.

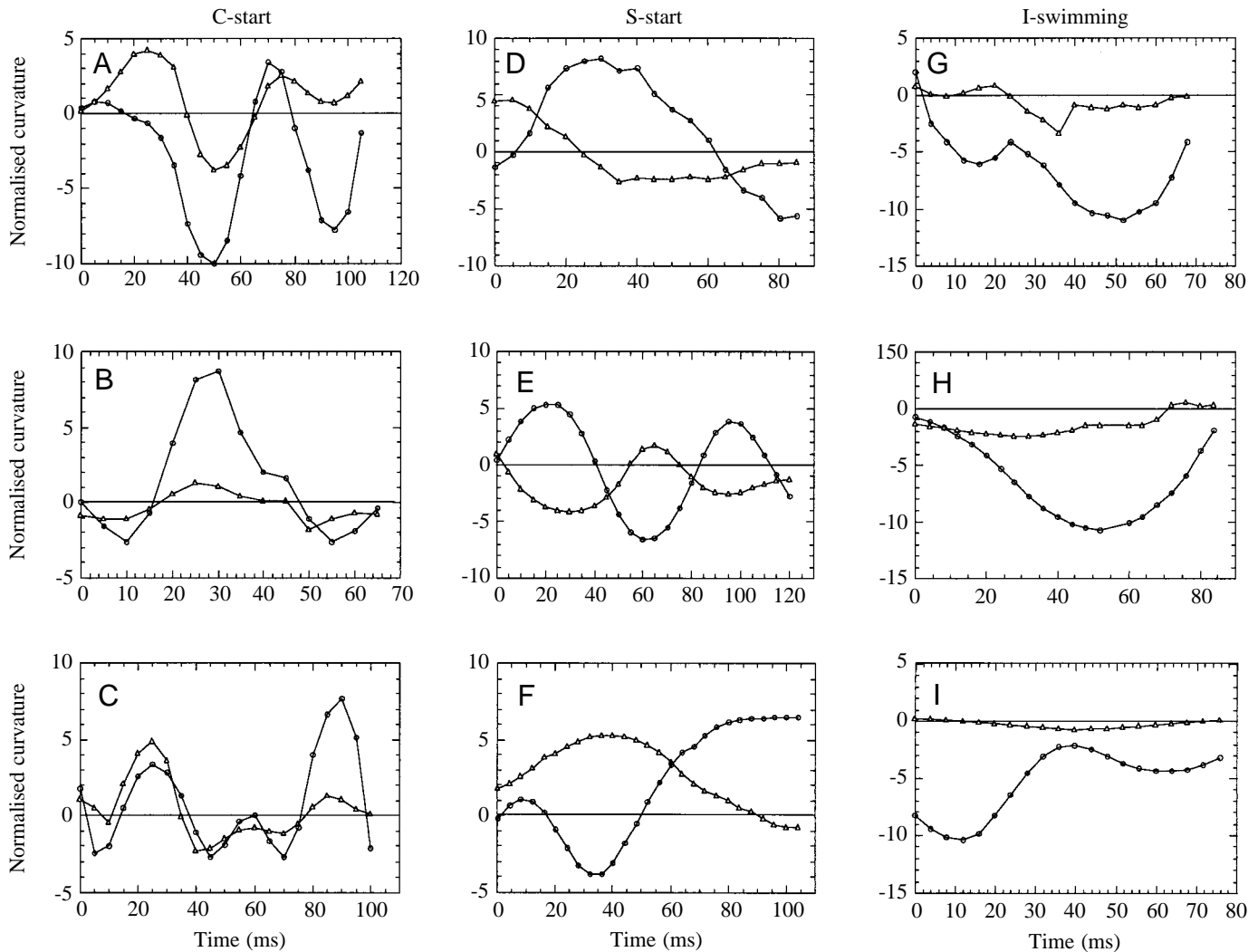


Fig. 5. Normalised curvature FL/R (where FL is fork length and R is local radius of curvature) of anterior (triangles) ($0.4 FL$) and posterior (circles) ($0.8 FL$) regions of the fish body during fast-starts. Curvature was positive for bending to the right and negative for bending to the left. When both anterior and posterior curvatures are zero, the fish is lying in a straight position. (A–C) C-starts. (D–F) S-start escape responses. (G–I) Intermediate fast-swimming movements (I-swimming). The sarcomere strains of red and white anterior and posterior muscle fibres on the left and right side of the fish body during these fast-starts are shown in Figs 7 and 8, respectively.

I-swimming

During I-swimming, the body curvatures were largest in the posterior region of the trunk. In this region, curvature amplitudes were similar to those of the C- and the S-start (see Fig. 5G–I). Hence, much larger sarcomere strains occurred posteriorly than anteriorly (see Figs 7G–I, 8G–I).

Strain variations in muscle fibres

Antero-posterior and red-white differences

Table 1 presents results from a statistical comparison of the maximum sarcomere strain at the convex side of the fish body. There was a large and significant difference ($P=0.0002$) between the maximum strains in red fibres (0.251 ± 0.126 , $N=48$) and white fibres (0.147 ± 0.074 , $N=48$). Strains for anterior fibres sampled at $0.4 FL$, which is close to ‘mid-body’, did not differ significantly from those for posterior fibres ($0.8 FL$).

C-start

Figs 7A–C and 8A–C show the sarcomere strain of red and white anterior and posterior muscle fibres on the left and right side of the fish body, respectively, during typical C-starts. No significant differences ($N=8$) in maximum sarcomere strain were found between red anterior (0.272 ± 0.211), red posterior (0.275 ± 0.120), white anterior (0.163 ± 0.142) and white posterior (0.168 ± 0.079 ; Table 1) fibres. On the basis of the curvature data shown in Fig. 5A–C, we conclude that in C-starts the maximum curvature does not consistently occur in the posterior or anterior half of the body, unlike S-starts and I-swimming.

S-start

Figs 7D–F and 8D–F show the sarcomere strain of the different muscle fibre types on the left and right side of the fish

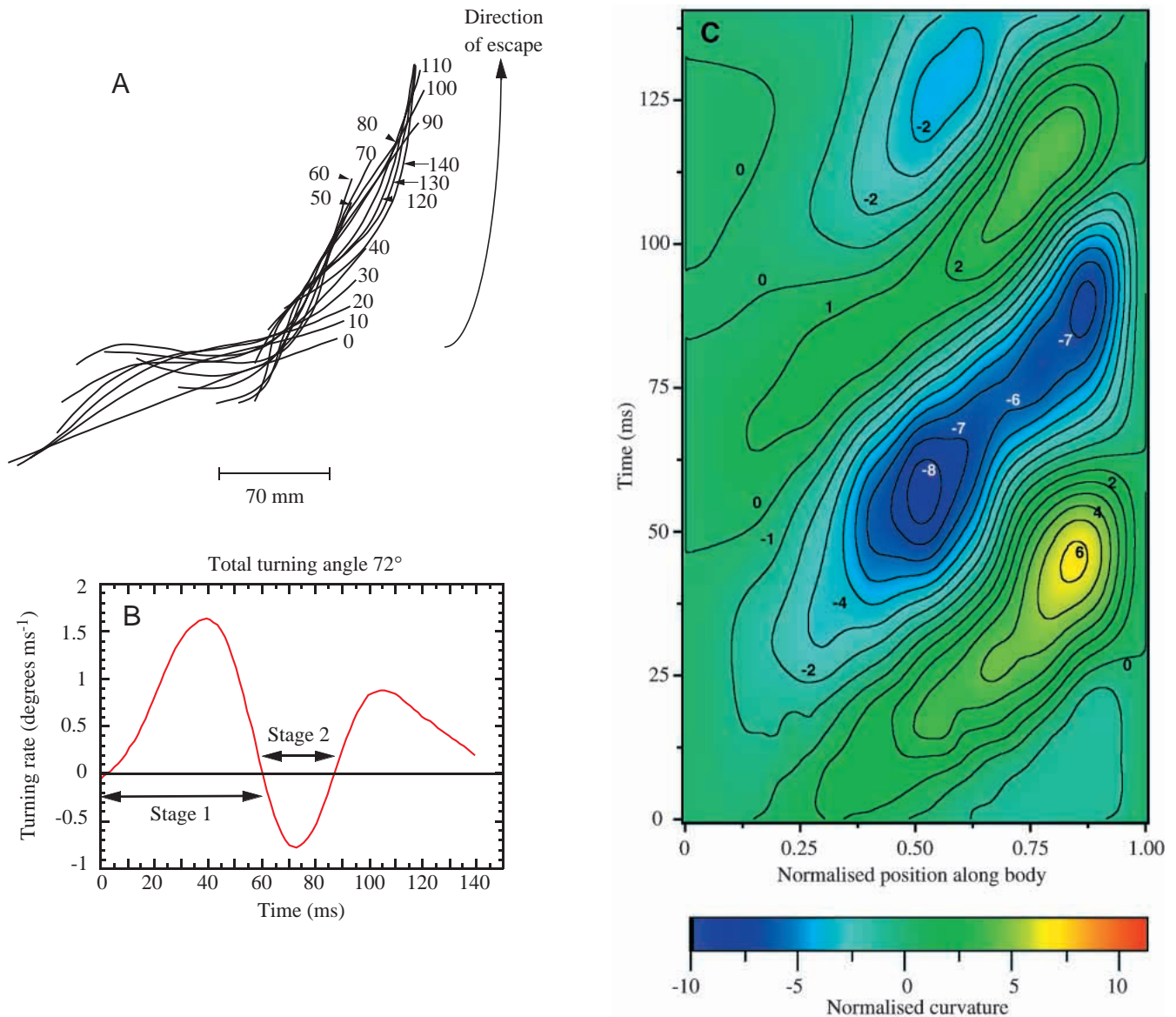


Fig. 6. S-start of an adult carp. (A) The central axis of the fish (plotted using the 31 points derived per calculated axis) during an S-start are shown every 10 ms. Times between tracings are in milliseconds from the first detectable movement. (B) The turning rate of the anterior body midline (snout to estimated centre of mass at $0.3 FL$, where FL is fork length) during this S-start. The stages of the start are indicated. (C) Contour plot of the body curvature during this S-start. The horizontal axis represents the body axis of the fish expressed as normalised FL (0 =tip of snout, 1 =fork of tail fin), the ordinate shows the time, and the colours and contours in the plot show the normalised curvature FL/R (where R is local radius of curvature). Curvature was positive for bending to the right and negative for bending to the left.

body, respectively, during S-starts. Red anterior (0.389 ± 0.019 , $N=8$) and white anterior (0.240 ± 0.017) fibres had significantly larger maximum strains than red posterior (0.171 ± 0.008) and white posterior (0.097 ± 0.004 ; Table 1) fibres, respectively. In general, during S-starts, red fibres had significantly larger maximum strains (0.280 ± 0.118 , $N=16$) than white fibres (0.167 ± 0.077 , $N=16$).

I-swimming

In Figs 7G–I and 8G–I, the sarcomere strain is shown during I-swimming on the left and right side of the fish body, respectively. During this swimming mode, only red posterior

fibres were exposed to significantly larger maximum strains (0.307 ± 0.053 , $N=8$) than all other muscle fibres (see Table 1). No significant differences in maximum strain were found between red and white fibres.

Comparison of different fast-starts

The maximum sarcomere strain of anterior fibres ($N=16$) was significantly larger during S-starts (0.315 ± 0.081) and C-starts (0.215 ± 0.16) than during I-swimming (0.103 ± 0.052). Posterior fibres were subjected to significantly larger maximum strains in I-swimming (0.242 ± 0.080) than in S-starts (0.134 ± 0.040).

Table 1. Mean maximum sarcomere strain during fast-starts

Muscle fibre type	N	Mean maximum sarcomere strain
Red, total	48	0.251±0.126 ^a
White, total	48	0.147±0.074 ^b
Anterior, total	48	0.209±0.138 ^a
Posterior, total	48	0.201±0.082 ^a
C, red anterior	8	0.272±0.211 ^a
C, red posterior	8	0.275±0.120 ^a
C, white anterior	8	0.163±0.142 ^a
C, white posterior	8	0.168±0.079 ^a
S, red anterior	8	0.389±0.019 ^a
S, red posterior	8	0.171±0.008 ^{bc}
S, white anterior	8	0.240±0.017 ^b
S, white posterior	8	0.097±0.004 ^c
I, red anterior	8	0.130±0.057 ^a
I, red posterior	8	0.307±0.053 ^b
I, white anterior	8	0.076±0.033 ^a
I, white posterior	8	0.177±0.032 ^a

Within each section of a column (separated by spaces), different letters (a,b,c) indicate a significant difference ($P \leq 0.05$).
N, total number of muscle tissue sections used for determining the mean maximum sarcomere strains (eight fish).
Values are means \pm s.d.
C, C-start; S, S-start; I, intermediate fast-swimming movements.

Discussion

Fast swimming movements of carp

Defining S-starts of carp

Predation S-starts are characterised by a variable S-shape of the fish axis, with the largest curvature and sarcomere strains located posteriorly and a small turning angle of the body. The (inclined) tail moves almost perpendicularly to the anterior axis of the fish (Hoogland et al., 1956). In escape S-starts, the largest sarcomere strains occur anteriorly and turning angles are generally larger. Webb (1976) reported such escape S-starts in large rainbow trout (*Oncorhynchus mykiss*) but with relatively small turning angles.

Comparing different fast-starts

The fast-starts investigated in the present study resulted from escape responses to the same stimulus. Why do carp respond to the same stimulus with a C-start in one case and with an S-start or I-swimming in other situations? It is interesting that the highest maximum strains were recorded for S-starts. It is thought that C-starts are initiated by the Mauthner system, but little is known about the mechanisms controlling S-starts. Depending on the stimulus, there is great variation in turning angle relative to the initial orientation of the fish (Domenici and Blake, 1993a). The maximum curvature of the anterior trunk during escape S-starts of carp in the present study was strikingly large compared with

predation S-starts of other species (during which larger posterior curvatures occur) and was associated with fairly large turning angles (approximately 60–80°). On the basis of these observations, it is expected that the final swimming direction can be determined least accurately in C-starts and most accurately in predation S-starts (in which precision of aiming is of vital importance). Escape S-starts seem to have an intermediate position in this respect.

During I-swimming, the largest curvatures and muscle strains occurred posteriorly, similar to the reported pattern for predation fast-starts. I-swimming is not a real fast-start but may occur just before or just after an actual fast-start.

The duration of C-starts is size-dependent (Domenici and Blake, 1993b) and linearly related to turning angle (Domenici and Blake, 1991; Domenici and Batty, 1994). C- and S-starts differ in their duration. Swimming performance is also influenced by water temperature and body length. In the present study, double-bend C-starts were performed slightly more quickly (50–100 ms) than S-starts or I-swimming. Fast-starts of rainbow trout with similar body sizes (20.4–29.6 cm TL) to our carp but at 15 °C had durations of 78–96 ms (Webb, 1976), whereas a duration of 115 ms was found for the fast-start of pike (*Esox* sp., 21.7 cm TL, 15 °C; Webb, 1978b). Given the large variation in results from previous studies on fast-starts, direct comparison between the performance of different species requires the use of more similar experimental designs.

Accelerations of the fish at 0.3 FL during fast-starts

The accelerations at 0.3 FL were larger during C-starts than during S-starts. The trough between the two main acceleration peaks observed during C-starts (Fig. 4A) was probably caused by rotation around the fish centre of mass at 0.3 FL, since bending caused the head and tail to move with large accelerations. During S-starts, maximum accelerations coincided with a tail-fin movement of high lateral velocity and at a considerable angle to the anterior axis of the fish, conditions for which a large thrust will be produced. Reported maximum accelerations during fast-starts vary greatly between different studies (for a review, see Domenici and Blake, 1997). When comparing accelerations during fast-starts from different fish species, factors such as fish size, water temperature and filming rate must be considered. The study of Harper and Blake (1990) is most appropriate for comparison with the present data because of their similar experimental conditions. In that study, overall mean maximum accelerations of $59.7 \pm 8.3 \text{ m s}^{-2}$ (mean ± 2 s.e.m., $N=30$) were reported for fast-starting rainbow trout (*Oncorhynchus mykiss*, 31.6 \pm 2 cm FL, mean ± 2 s.e.m.) and much higher single maximum accelerations (96 m s^{-2}) compared with those in the present study (approximately 54 m s^{-2} for C-starts and 40 m s^{-2} for S-starts).

Sarcomere strains during different fast-starts

It is assumed that the strains of red muscle fibres depend on (1) the distance between the fibre and the backbone of the fish and (2) the instantaneous local curvature of the body during

swimming. This is supported by a study of Coughlin et al. (1996), who compared calculated and measured strain in scup (*Stenotomus chrysops*). Strain variations of white fibres are, because of their helical fibre paths, dependent not only on their distance to the body axis but also on their orientation. Red fibres are consequently exposed to larger strains, as was found in the present study (e.g. 25.1% for red fibres and 14.7% for white fibres). Strains determined by Rome and Sosnicki (1991) in rigor muscle of carp (*Cyprinus carpio*, at 0.38 and 0.68 TL) that had been bent into extreme curvatures similar to those found during C-starts also showed larger maximum strain values in red than in white fibres. They found the highest sarcomere strains in red anterior fibres (up to 25%, compared with 16.5% for red posterior fibres), which they attributed to the relatively large distance between these fibres and the body axis. In the present study, maximum strains of red anterior and posterior fibres during C-starts were similar, approximately 27%. Rome et al. (1988) obtained a maximum shortening

velocity (V_{\max}) of $4.65 \pm 0.55 L s^{-1}$ (where L is length, mean \pm S.E.M., $N=5$) for red muscle fibres and $12.88 \pm 0.5 L s^{-1}$ for skinned white fibres ($N=6$) both at 15 °C. Since our experiments were carried out at a higher temperature (23 °C), we expect somewhat higher values than those obtained by Rome et al. (1988): approximately $5.5 L s^{-1}$ for red muscle fibres and $15 L s^{-1}$ for white muscle fibres. Owing to the low V_{\max} of red fibres compared with the fast white fibres, red fibres are not able to equal the high shortening velocity of white fibres during very rapid fast-starts and will therefore tend to buckle on the concave side of the fish body. This confirms earlier suggestions by Rome et al. (1988) and Rome and Sosnicki (1991). The negative sarcomere strains of red fibres shown in Figs 7 and 8 were not corrected for these buckling effects, but reflect the shortening that these fibres would need to undergo to avoid buckling. White posterior fibres experienced similar strains (16.8%) to white anterior fibres (16.3%) during C-starts. Rome and Sosnicki (1991) found that white posterior

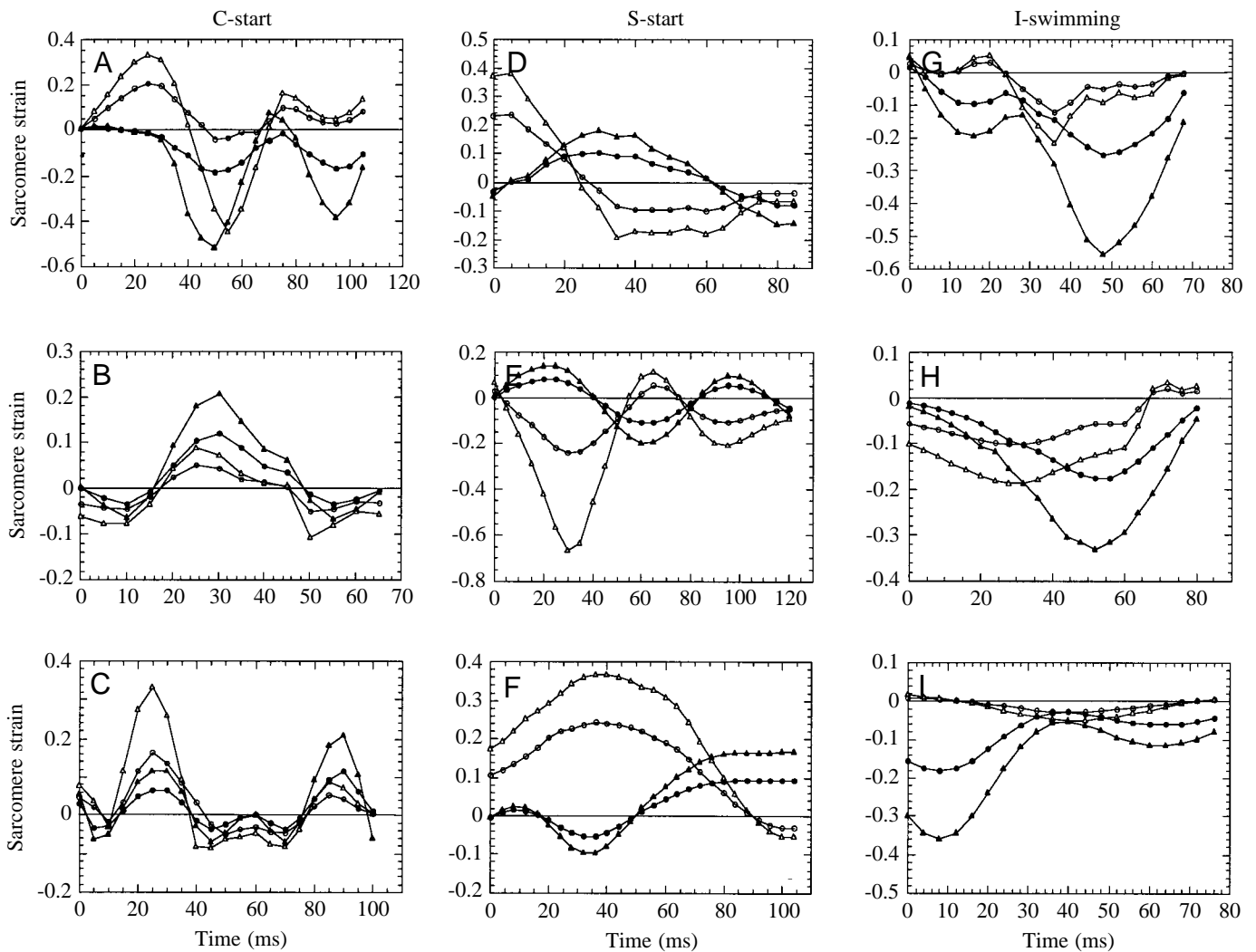


Fig. 7. Sarcomere strain of red (triangles) and white (circles) anterior (open symbols) and posterior (filled symbols) muscle fibres on the left side of the fish body during fast-starts. Positive strains indicate muscle fibre lengthening; negative strains indicate muscle fibre shortening. (A–C) C-starts. (D–F) S-start escape responses. (G–I) Intermediate fast-swimming movements (I-swimming).

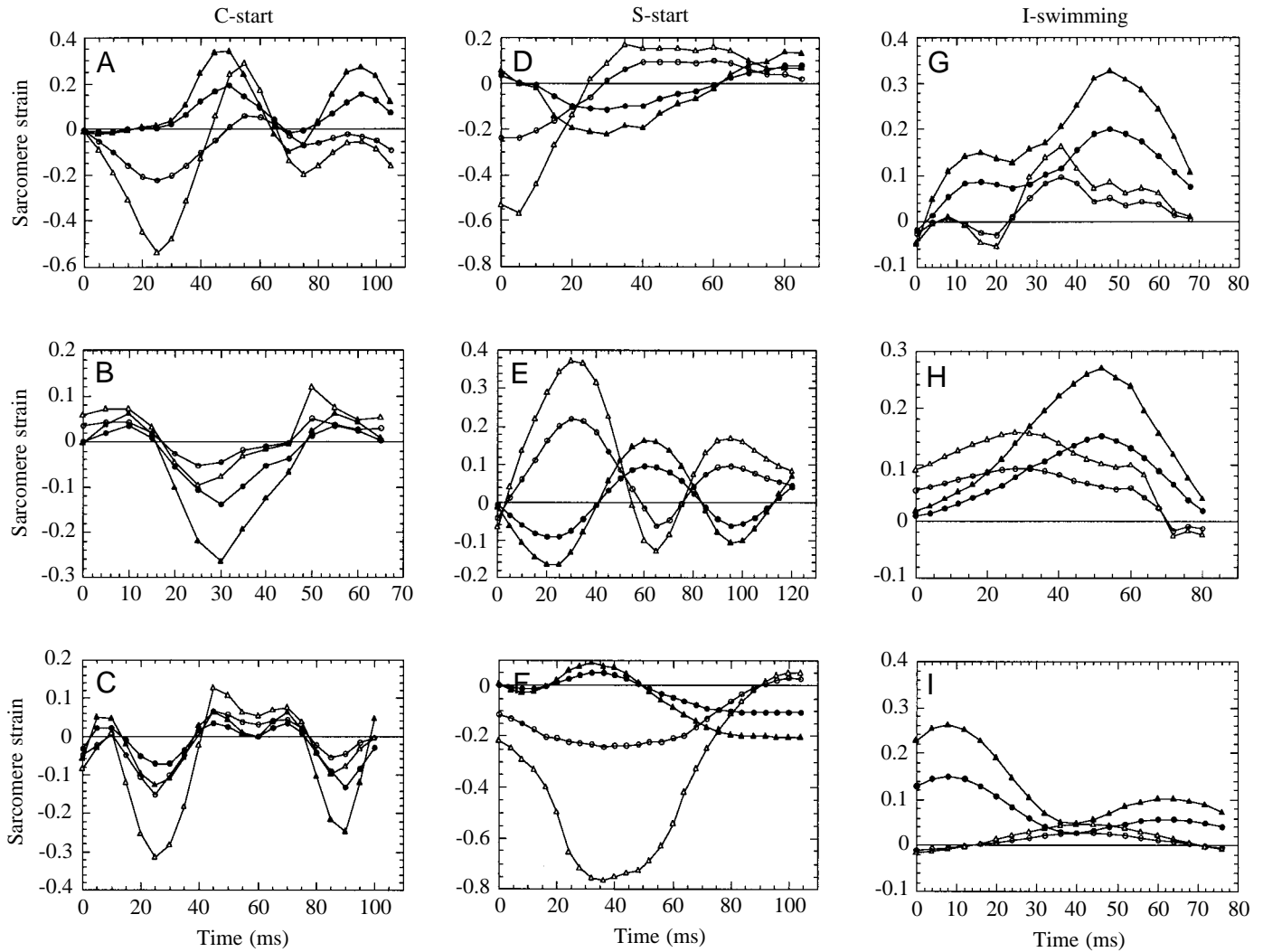


Fig. 8. Sarcomere strain of red (triangles) and white (circles) anterior (open symbols) and posterior (filled symbols) muscle fibres on the right side of the fish body during fast-starts. Positive strains indicate muscle fibre lengthening; negative strains indicate muscle fibre shortening. (A–C) C-starts. (D–F) S-start escape responses. (G–I) Intermediate fast-swimming movements (I-swimming).

fibres experienced larger strains than white anterior fibres (anterior 6.1%; posterior 10.7%) but with lower values than in our study. The carp we investigated were larger (22.5–27.5 cm *FL*) than those of Rome and Sosnicki (1991) (10–20 cm *TL*). The sarcomere strains we found in anterior fibres during S-starts were more than twice as large as in posterior fibres for both red and white muscle fibres (Table 1), owing to the larger anterior curvature that occurs in S-starts relative to C-starts. The maximum strain rate we calculated was less than approximately 10.5 s^{-1} for white fibres and 35 s^{-1} for red fibres.

Sarcomere strain in relation to titin isoforms

Sarcomere strain variations during cyclic swimming are smaller for white fibres than for red fibres (Rome et al., 1988; van Leeuwen et al., 1990; Rome and Sosnicki, 1991). van Leeuwen et al. (1990) and van Leeuwen (1992) calculated strains of approximately 1.5–2% and 5% for white and red

axial muscle fibres, respectively, of *Cyprinus carpio* during cyclic swimming. Posterior fibres experienced larger sarcomere strains than did anterior fibres during cyclic swimming (van Leeuwen, 1995). van Leeuwen et al. (1990) found that, during cyclic swimming, anterior fibres were mainly concentrically active, within a limited length range, whereas fibres in the caudal peduncle were active for a longer period while being stretched. At the level of the anus, the concentric and eccentric activation periods were approximately equal. Rome and Sosnicki (1991) determined strains in rigor muscle of carp with body postures similar to those of cyclic swimming. They found strains of 2.9% anteriorly (at 0.38 *TL*) and 5.7% posteriorly (at 0.68 *TL*). For intermittent swimming, large strains (up to 20%) were calculated for posterior fibres of carp (van Leeuwen et al., 1990; for a correction, see also van Leeuwen, 1992). For cyclic swimming, we found that the combined effects of muscle fibre type and muscle location led to the following set of declining mean sarcomere strains ($N=8$):

red posterior 0.051 ± 0.023 ; white posterior 0.028 ± 0.013 ; red anterior 0.02 ± 0.022 ; white anterior 0.012 ± 0.012 . The observed variation in strain corresponds well with previously reported differences in molecular mass of the huge, highly elastic, muscle protein titin: red and posterior fibres of carp possessed larger titin isoforms compared with white and anterior fibres (Spierts et al., 1997). The increased molecular mass of titin correlates with an increase in the length of the highly elastic segment of titin (I-band segment). The position of titin in a slack sarcomere is illustrated in Fig. 1A. Titin acts as a dual spring resisting both negative (Fig. 1B and the green curve in Fig. 1D) and positive (Fig. 1C and the red curves in Fig. 1D) sarcomere strain. Differences in the length of the highly elastic titin segment are reflected in differences in the passive tension *versus* sarcomere length relationship of skinned muscle fibres (Granzier et al., 1996). When red fibres are gradually stretched at a constant velocity from resting length to twice this length, the passive tension *versus* sarcomere length curve increases more steeply in fibres with small titin isoforms (anterior fibres) than in fibres with larger titin isoforms (posterior fibres). The passive tension *versus* sarcomere length curves for carp red anterior and posterior fibres upon stretching and shortening, derived from Spierts et al. (1997), are shown in Fig. 1D as the red and green curves, respectively, expressed relative to a maximum active tension of approximately 150 kPa. The smaller titin isoform in anterior fibres results in greater passive tension for a given sarcomere strain. Spierts et al. (1997) hypothesised that sarcomere strain is one of the functional variables that modulates the expression of different titin isoforms in axial muscle fibres of carp, thus reducing energy loss during cyclic loading of the muscle fibres. In carp, the fibres that experience the largest sarcomere strains during cyclic and intermittent swimming are those reported to have the largest titin isoforms, allowing these fibres to attain large strain amplitudes with relatively low tensions.

Fig. 1D shows the mean maximum sarcomere length excursions of red (25.1%, dashed lines) and white (14.7%, solid lines) muscle fibres of carp during fast-starts in a normalised force *versus* sarcomere length curve. The blue dashed line indicates a hypothetical work loop for the white muscles that power the fast-start (see also the work loops in Fig. 4 of Johnston et al., 1995). The white muscle fibres start to shorten at slack length ($1.95 \mu\text{m}$) to approximately $1.66 \mu\text{m}$ and generate approximately 45–50% maximum tension. During (passive) muscle lengthening, the work loop 'follows' the matching passive tension *versus* sarcomere length curve (not indicated for white muscles in Fig. 1D). If the fast-starts were powered by red muscles, these fibres would need to shorten to approximately $1.44 \mu\text{m}$, a sarcomere length at which the tension generated is very low and the fibres might be damaged. Red fibres, however, are not able to match the high shortening velocity of white fibres and are protected from being damaged by buckling on the concave side of the fish body (shaded area in Fig. 1D). The largest loading of titin probably occurs during fast-starts in red fibres at approximately $0.4FL$ at the point at which the largest strains occur and at

which the smallest titin isoforms are found. To quantify the passive tension required to stretch red anterior fibres maximally during S-starts, we compared our strain value of 39% with the passive tension of carp red anterior fibres derived from a passive tension *versus* sarcomere length curve (Fig. 2A in Spierts et al., 1997). The passive tension necessary for a strain of 39% in these fibres is 20 kPa (Spierts et al., 1997). Of this 20 kPa, the titin-based passive tension is 14 kPa, whereas the intermediate-filament-based passive tension is 6 kPa. This passive tension during stretching is considerable compared with the maximum active tension that can be generated by carp red muscles (which is low because of the buckling described above) when these fibres actively participate in power generation during fast-starts. The passive tension of red fibres during shortening, however, is much smaller, also because of this buckling. Further research is required to quantify the energetic consequences of these features of muscle.

We thank Dr H. A. Akster and Professor Dr J. W. M. Osse for useful discussions and comments on the manuscript. We also thank an anonymous referee for a detailed report that helped to improve this paper. This research was supported by the Life Sciences Foundation (SLW), which is subsidised by the Netherlands Organisation for Scientific Research (NWO).

References

- Akster, H. A.** (1985). Morphometry of muscle fibre types in the carp (*Cyprinus carpio* L.): relationships between structural and contractile characteristics. *Cell Tissue Res.* **241**, 193–201.
- Alexander, R. McN.** (1969). The orientation of muscle fibres in the myomeres of fishes. *J. Mar. Biol. Ass.* **49**, 263–290.
- Coughlin, D. J., Valdes, L. and Rome, L. C.** (1996). Muscle length changes during swimming in scup: sonomicrometry verifies the anatomical high-speed cine technique. *J. Exp. Biol.* **199**, 459–463.
- de Boor, C.** (1978). *A Practical Guide to Splines*. Berlin: Springer.
- Domenici, P. and Batty, R. S.** (1994). Escape manoeuvres of schooling *Clupea harengus*. *J. Fish Biol.* **45** (Suppl. A) 97–110.
- Domenici, P. and Blake, R. W.** (1991). The kinematics and performance of the escape response in the angelfish (*Pterophyllum eimekei*). *J. Exp. Biol.* **156**, 187–205.
- Domenici, P. and Blake, R. W.** (1993a). Escape trajectories in angelfish (*Pterophyllum eimekei*). *J. Exp. Biol.* **177**, 253–272.
- Domenici, P. and Blake, R. W.** (1993b). The effect of size on the kinematics and performance of angelfish (*Pterophyllum eimekei*) escape responses. *Can. J. Zool.* **71**, 2319–2326.
- Domenici, P. and Blake, R. W.** (1997). The kinematics and performance of fish fast-start swimming. *J. Exp. Biol.* **200**, 1165–1178.
- Eaton, R. C., Bombardiere, R. A. and Meyer, D. L.** (1977). The Mauthner-initiated startle response in teleost fish. *J. Exp. Biol.* **66**, 65–85.
- Frith, H. R. and Blake, R. W.** (1991). Mechanisms in the startle response in the northern pike, *Esox lucius*. *Can. J. Zool.* **69**, 2831–2839.
- Fürst, D. O., Osborne M., Nave R. and Weber, K.** (1988). The organisation of titin filaments in the half-sarcomere revealed by monoclonal antibodies in immunoelectron microscopy: a map of

- ten nonrepetitive epitopes starting at the Z-line extends close to the M-line. *J. Cell Biol.* **106**, 1563–1572.
- Granzier H. L. M., Helmes M. and Trombitás, K.** (1996). Nonuniform elasticity of titin in cardiac myocytes: a study using immunoelectron microscopy and cellular mechanics. *Biophys. J.* **70**, 430–442.
- Harper, D. G. and Blake, R. W.** (1990). Fast-start performance of rainbow trout *Salmo gairdneri* and northern pike *Esox lucius*. *J. Exp. Biol.* **150**, 321–342.
- Hertel, H.** (1966). *Structure, Form and Movement*. New York: Reinhold Publishing Corp. 251pp.
- Hoogland, R., Morris, D. and Tinbergen, N.** (1956). The spines of sticklebacks (*Gasterosteus* and *Pygosteus*) as a means of defence against predators (*Perca* and *Esox*). *Behaviour* **10**, 205–236.
- Johnston, I. A., van Leeuwen, J. L., Davies, M. L. F. and Beddow, T.** (1995). How fish power predation fast-starts. *J. Exp. Biol.* **198**, 1851–1861.
- Kasapi, M. A., Domenici, P., Blake, R. W. and Harper, D.** (1993). The kinematics and performance of escape responses of the knifefish *Xenomystus nigri*. *Can. J. Zool.* **71**, 189–195.
- Kimmel, C. B., Eaton, R. C. and Powell, S. L.** (1980). Decreased fast-start performance of zebrafish larvae lacking Mauthner neurons. *J. Comp. Physiol.* **140**, 343–351.
- Lipschutz, M. M.** (1969). *Theory and Problems of Differential Geometry*. *Schaum's Outline Series*. New York: McGraw-Hill. 269pp.
- Maruyama, K.** (1986). Connectin, an elastic filamentous protein of striated muscle. *Int. Rev. Cytol.* **104**, 81–114.
- Maruyama, K.** (1994). Connectin, an elastic protein of striated muscle. *Biophys. Chem.* **50**, 73–85.
- Page, S. G. and Huxley, H. E.** (1963). Filament lengths in striated muscle. *J. Cell Biol.* **19**, 369–390.
- Rohlf, F. J. and Sokal, R. R.** (1981). *Statistical Tables*, second edition. New York: W.H. Freeman & Company. 219pp.
- Rome, L. C., Funke, R. P., Alexander, R. McN., Lutz, G., Aldridge, H., Scott, F. and Freadman, M.** (1988). Why animals have different muscle fibre types. *Nature* **335**, 824–827.
- Rome, L. C. and Sosnicki, A. A.** (1991). Myofilament overlap in swimming carp. II. Sarcomere length changes during swimming. *Am. Physiol. Soc.* **260**, 289–296.
- Shapiro, S. S. and Wilk, M. B.** (1965). An analysis of variance test for normality (complete samples). *Biometrika* **52**, 591–611.
- Sokal, R. R. and Rohlf, F. J.** (1981). *Biometry*, second edition. New York: W. H. Freeman & Company. 859pp.
- Spierts, I. L. Y., Akster, H. A. and Granzier, H. L.** (1997). Expression of titin isoforms in red and white muscle fibres of carp (*Cyprinus carpio* L.) exposed to different sarcomere strains during swimming. *J. Comp. Physiol. B* **167**, 543–551.
- van Leeuwen, J. L.** (1992). Muscle function in locomotion. In *Mechanics of Animal Locomotion* (ed. R. McN. Alexander). *Adv. Comp. Env. Physiol.* **11**, 191–250.
- van Leeuwen, J. L.** (1995). The action of muscles in swimming fish. *Exp. Physiol.* **80**, 177–191.
- van Leeuwen, J. L., Lankheet, M. J. M., Akster, H. A. and Osse, J. W. M.** (1990). Function of red axial muscles of carp (*Cyprinus carpio*): recruitment and normalised power output during swimming in different modes. *J. Zool., Lond.* **220**, 123–145.
- Wang, K.** (1985). Sarcomere associated cytoskeletal lattices in striated muscle. Review and hypothesis. In *Cell and Muscle Motility 6* (ed. J. W. Shay), pp. 315–369. New York: Plenum Publishing Company.
- Wang K., McCarter R., Wright J., Beverly J. and Ramírez-Mitchell R.** (1991). Regulation of skeletal muscle stiffness and elasticity by titin isoforms: a test of the segmental extension model of resting tension. *Proc. Natl. Acad. Sci. USA* **88**, 7101–7105.
- Wang K., McCarter R., Wright J., Beverly J. and Ramírez-Mitchell R.** (1993). Viscoelasticity of the sarcomere matrix of skeletal muscles. The titin–myosin composite is a dual-stage molecular spring. *Biophys. J.* **64**, 1161–1177.
- Webb, P. W.** (1975). Acceleration performance of rainbow trout *Salmo gairdneri* and green sunfish *Lepomis cyanellus*. *J. Exp. Biol.* **63**, 451–465.
- Webb, P. W.** (1976). The effect of size on the fast-start performance of rainbow trout *Salmo gairdneri* and a consideration of piscivorous predator–prey interactions. *J. Exp. Biol.* **65**, 157–177.
- Webb, P. W.** (1978a). Effects of temperature on fast-start performance of rainbow trout, *Salmo gairdneri*. *J. Fish. Res. Bd Can.* **35**, 1417–1422.
- Webb, P. W.** (1978b). Fast-start performance and body form in seven species of teleost fish. *J. Exp. Biol.* **74**, 211–226.
- Webb, P. W. and Blake, R. W.** (1985). Swimming. In *Functional Vertebrate Morphology* (ed. M. Hildebrand, D. M. Bramble, K. Liem and D. B. Wake), pp. 110–128. Cambridge: Harvard University Press.
- Weihls, D.** (1973). The mechanism of rapid starting of slender fish. *Biorheology* **10**, 343–350.
- Woltring, H.** (1986). A Fortran package for generalised, cross-validatory spline smoothing and differentiation. *Adv. Engng Software* **8**, 104–113.